

Magnetic phase transitions induced by pressure and magnetic field: The case of antiferromagnetic USb₂

Leonid Sandratskii

Max Planck Institute of Microstructure Physics, D-06120 Halle, Germany

(Received 30 December 2018; revised manuscript received 22 February 2019; published 11 March 2019)

Fascinating phenomena observed under applied pressure and magnetic field are attracting much research attention. Recent experiments have shown that application of the pressure or magnetic field to the USb₂ compound induce the transformations of the ground-state antiferromagnetic (AFM) structure (+ - -+) to, respectively, ferromagnetic (FM) or ferrimagnetic structures. Remarkably, the magnetic critical temperature of the FM state, induced by pressure, is more than two times smaller than the Néel temperature of the AFM ground state. We performed density-functional theory (DFT) and DFT+*U* studies to reveal the origin of the unusual magnetic ground state of the system and the driving mechanisms of the phase transitions. We investigate both the magnetic anisotropy properties and the parameters of the interatomic exchange interactions. To study pressure-induced effects we carry out calculations for reduced volume and demonstrate that the existence of the AFM-FM phase transformation depends on the peculiar features of the magnetic anisotropy. We discuss why the magnetic field that couples directly to the magnetic moments of atoms leads to the phase transition to the ferrimagnetic state whereas the pressure that does not couple directly to magnetic moments results in the FM structure. Our work demonstrates how the competition of different physical factors leads to variety of unusual properties of the antiferromagnetic USb₂.

DOI: [10.1103/PhysRevB.99.094411](https://doi.org/10.1103/PhysRevB.99.094411)

I. INTRODUCTION

The wide variety of physical properties observed in uranium compounds [1] has been attracting much research attention to this class of materials. Several factors are responsible for the broad spectrum of properties. One of the important factors is the different degree of localization of the U 5*f* electrons extending from very strong in, e.g., UPd₃ [2] to relatively weak in, e.g., U₂Ni₂₁B₆ [3]. Another important factor is the large spin-orbit coupling (SOC) of the 5*f* electrons that leads to strong competition of the SOC-caused properties such as magnetic anisotropy (MA) and Dzyaloshinskii-Moriya interaction (DMI) and the properties whose appearance is not linked to the presence of the SOC such as isotropic exchange interaction of the Heisenberg type. Because of moderate values of the magnetic interactions in the uranium compounds the external pressure and magnetic field reachable in the modern laboratories are sufficient to initiate various phase transformations [4–8] whose understanding is an important tool to gain deeper insight into diverse physics of the systems.

This paper deals with the USb₂ compound where recent high-pressure [9] and high-magnetic field [10] experiments revealed nontrivial phase transformations. The USb₂ has the crystal structure of the anti-Cu₂Sb (Fig. 1) type where the uranium atoms form layers parallel to the crystallographic *ab* plane separated by the layers of Sb atoms [11]. The ground state of USb₂ is a rather special (+ - -+) antiferromagnetic structure (Fig. 1) that is different from a simpler (+ - +-) AFM structure observed in the related UBi₂ compound [11]. Here “+” and “-” denote the directions of the atomic moments of the uranium layers parallel and antiparallel to the *c* axis, respectively. Within each layer the atomic moments are

parallel to each other. The Néel temperature of USb₂ at the ambient conditions is about 200 K [12].

The Fermi surface of USb₂ was studied in de Haas–van Alphen and Shubnikov–de Haas experiments [13,14]. The cylindrical form of the Fermi surface was found which was explained by the layered type of the crystal and magnetic structure. The first-principle density-functional theory (DFT) calculation of the band structure and Fermi surface of USb₂ was reported in Ref. [15]. This calculation has shown that in the band structure there are states characterized by strong hybridization of the U 5*f* and Sb 5*p* atomic orbitals as well as the U 5*f* states with a small admixture of the Sb 5*p* orbitals. The cylindrical form of the sheets of the calculated Fermi surface compares well with the experiment.

An early angle-resolved photoemission spectroscopy (ARPES) study [12] has shown the dispersion of a narrow feature near the Fermi level that was present also in the normal emission experiment. This result reveals that the electronic structure of USb₂ has three-dimensional (3D) character that is in contrast to the definitely 2D character of the Fermi surface proposed in Refs. [13,14]. In a later high-resolution ARPES study, a kink in the 5*f*-band dispersion was observed showing the itinerant character of the 5*f* electrons and importance of the electron correlations [16].

As mentioned above, this paper was motivated by recent experiments under pressure and magnetic field that revealed interesting magnetic phase transformations. The applied pressure leads to the first-order-type magnetic phase transition with the new magnetic state identified as ferromagnetic [9]. In the AFM phase, the increasing pressure leads to a monotonic increase of the Néel temperature up to about 240 K.

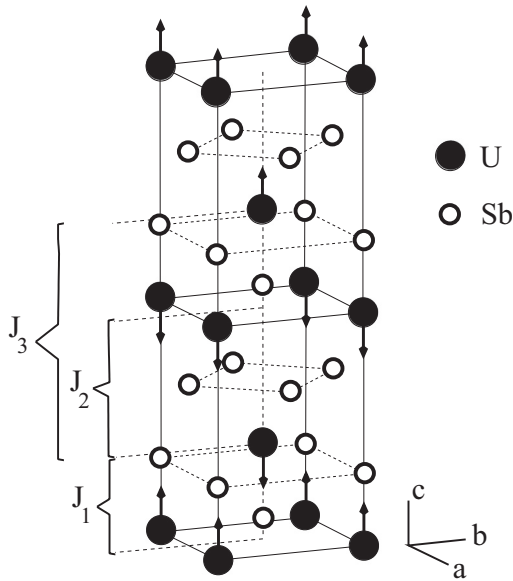


FIG. 1. Magnetic unit cell of the $(+ - - +)$ magnetic structure. J_1, J_2, J_3 are exchange parameters between corresponding layers of U atoms.

Remarkably, immediately after the transition to the ferromagnetic (FM) state the magnetic critical temperature (T_{cr}) drops more than two times to about 90 K.

The application of the magnetic field also leads to the phase transition that was identified as the transition to the ferrimagnetic (FiM) state of the $(+ + + -)$ type [10]. It is worth emphasizing that according to this experiment the magnetic field that couples directly to magnetic moments leads to the reversal of only one of the two antiparallel atomic moments in the magnetic unit cell whereas the pressure that does not directly couple to the atomic moments results in the FM structure with all uranium moments being parallel.

The combination of the experimental properties including a special $(+ - - +)$ ground-state magnetic structure, the phase transitions to two different uncompensated magnetic structures induced by pressure and magnetic field, and strong drop of the critical temperature in the FM phase compared to the ground-state AFM phase reveal the competition of various physical trends and make USb_2 a very interesting object of theoretical study.

A microscopic mechanism of the unusual antiferromagnetic order and pressure-induced antiferromagnetic (AFM)-FM transition was discussed in Ref. [17]. A relatively simple model was considered where the 3D crystal was replaced by a film parallel to the ab plane and containing three layers of the U atoms. In the mathematical treatment these three layers were considered as two overlapping subsystems containing two U layers each. The Hamiltonian of the minimal model used in Ref. [17] depends on a number of parameters specifying the energy of the U $5f$ level, on-site Coulomb interaction of the U $5f$ electrons, intersite hopping of the Sb electrons, relative shift of the bands of two inequivalent Sb bands, the number of electrons, and the hybridization between U $5f$ and conduction-electron states. The effect of pressure was introduced through the variation of the hybridization

parameter and the energy of the U $5f$ level. It was shown that within this model the transition from the AFM to FM state can be obtained.

The goal of the present paper is to advance the understanding of the intriguing physics of the USb_2 compound on the basis of the DFT-based calculations. The calculations are performed for the variety of magnetic configurations allowing us to address experimental phase transitions and extract valuable information about underlying magnetic interactions. To investigate the role of the intra-atomic electron correlations we employ the local-density approximation plus U (LDA+ U) method. To address the high-pressure and high-field experiments we perform calculations with reduced crystal volume and applied magnetic field, respectively.

The paper is organized as follows. In Sec. II we discuss computational details. Section III presents the results of the calculations: Secs. III A and III B consider the magnetic structures collinear to the c axis for both ambient [18] and contracted lattices, Sec. III C deals with the magnetic anisotropy properties, Sec. III D presents calculated exchange parameters and discusses the properties of the critical temperatures, and Sec. III E describes the results of in-field calculations. In Sec. IV the conclusions of the paper are formulated.

II. COMPUTATIONAL DETAILS

The calculations are performed with the augmented spherical waves (ASWs) method [19,20] generalized to deal with noncollinear magnetism, spin-orbit coupling, and applied magnetic field [21,22]. Both LDA [23] and LDA+ U [24,25] approaches are used [26]. It is known that the LDA has limitations in the description of the uranium compounds. For example, the LDA underestimates the values of atomic-orbital moments [27,28]. Several approaches were suggested to deal with this LDA shortcoming. One of the approaches consists in adding so-called orbital polarization terms to the energy functional and Kohn-Sham equation [29]. Many calculations were performed using this approach (see, e.g., [28–33]). This somewhat empirical method allowed us to considerably improve the agreement between calculations and experiments.

A better founded approach to improve the LDA performance is the LDA+ U method designed for a more consequent account for the intra-atomic electronic correlations [24–26]. In this paper we employ the LDA+ U method in the form suggested by Dudarev *et al.* [34]. The method results in the $m\sigma$ dependent potential where m is magnetic quantum number and σ is the spin projection. The potential experienced by $m\sigma$ orbital depends on the occupation matrix $n_{m\sigma, m'\sigma}$ and is self-consistently determined in the LDA+ U calculations. As a trend, a higher occupation of a $m\sigma$ orbital leads to a deeper potential for this orbital stimulating an enhancement of the orbital moment. In this respect there is an analogy with the orbital polarization correction approach [29].

In the calculations we used experimental lattice parameters given in Ref. [11]. The mesh of \mathbf{k} points in the Brillouin zone was $20 \times 20 \times 8$ for the unit cell containing two layers of uranium atoms and $20 \times 20 \times 4$ for the unit cell with four layers of uranium atoms.

To study the effect of pressure we performed calculations with reduced volume. The magnetic field enters the

calculations through the Zeeman term with field acting on both spin and orbital magnetic moments [35].

III. RESULTS

A. Magnetic states collinear to the c axis at ambient pressure

We begin with the study of a number of magnetic configurations $(+ - - +)$, $(+ - + -)$, $(+ + - -)$, $(+ + + -)$, $(+ + + +)$ with atomic moments collinear to the c axis. We will use for these structures the notations AFM-II, AFM-I, AFM-III, FiM, FM, respectively. These magnetic states were selected as relevant to the experimental findings. The results of the LDA calculations for the ambient lattice parameters are given in Table I.

As seen from the second column of Table I, the LDA calculations give the antiferromagnetic AFM-I structure as the lowest in energy. The experimental magnetic ground-state AFM-II has somewhat higher energy. The energy increases for AFM-III, FiM, and FM configurations. The competition of the energies of the AFM-I and AFM-II magnetic structures is not unexpected taking into account that the experimental ground state of the related compound UBi_2 is AFM-I. Obviously, in the case of USb_2 the LDA calculations do not reproduce correctly the result of the competition between the energies of the AFM-I and AFM-II structures.

Also the value of the atomic moment of the AFM-II structure is considerably lower than the experimental value of $1.88\mu_B$ [11]. In Table I we present calculated spin, orbital, and total moments of the U atoms. As expected from the third Hund's rule, in the case of the U atom the directions of the spin and orbital moments are opposite. The values of the atomic moments depend on the magnetic structure. However, this dependence is moderate. For example, the total moment varies from $1.04\mu_B$ to $1.15\mu_B$ remaining in all cases distinctly smaller than the experimental value of the moment.

Aiming at solving the problems of LDA, we performed calculations with the LDA+ U method. In Fig. 2 we compare the U 5*f* densities of states (DOS) calculated with LDA and LDA+ U methods for the AFM-II configuration of atomic moments. The results shown in the figure are obtained for the ambient lattice and parameter $U = 100$ mRy. There is clear

TABLE I. The energies and atomic magnetic moments of several magnetic states collinear to the c axis. The LDA calculations are performed for ambient lattice. The energy origin is at the energy of the $(+ - - +)$ structure. In the case of $(+ + + -)$ structure the U atoms are not equivalent to each other and have somewhat different magnetic moments. In the table an average value of the atomic moment is given. The negative values of the spin moments emphasize their opposite direction with respect to the orbital and total moments.

Magnetic structure	Energy (mRy/U at)	Atomic moments in μ_B		
		spin	orbital	total
AFM-II	0	-1.68	2.83	1.15
AFM-I	-0.229	-1.69	2.81	1.12
AFM-III	0.386	-1.59	2.63	1.04
FiM	0.265	-1.62	2.72	1.10
FM	0.895	-1.55	2.64	1.09

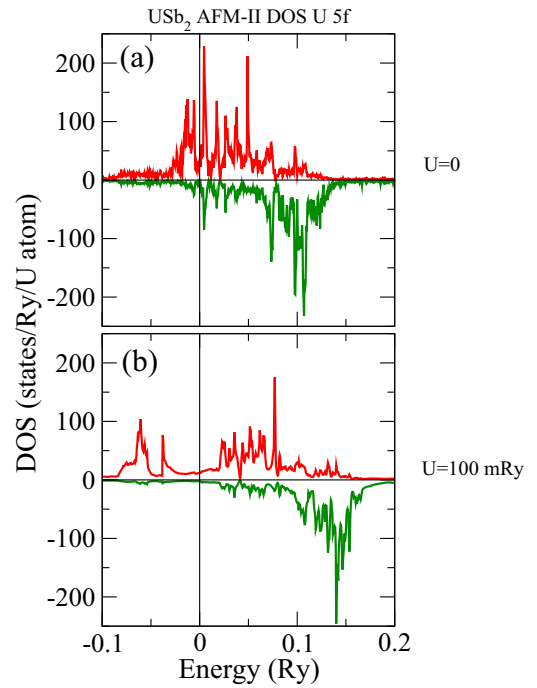


FIG. 2. The U 5*f* density of states of the AFM-II configuration calculated with LDA (a) and LDA+ U (b) methods. The results shown in this figure are obtained for the experimental ambient lattice parameters. Parameter $U = 100$ mRy. The positive curves present the spin-up DOS, the negative curves present the spin-down DOS. The c axis is the axis of spin quantization. The energy origin is at the Fermi level.

trend to the lower energy of the occupied states and higher energy of the empty states.

The LDA+ U calculations were performed for several U values. The data obtained in the calculations are presented in Fig. 3. The absolute values of both spin and orbital moments increase with increasing U . The increase of the magnitude of the orbital moment is distinctly faster than the increase of the spin moment resulting in monotonic increase of the total moment as a function of U . The uranium atomic moments close to the experimental moment are obtained for the U

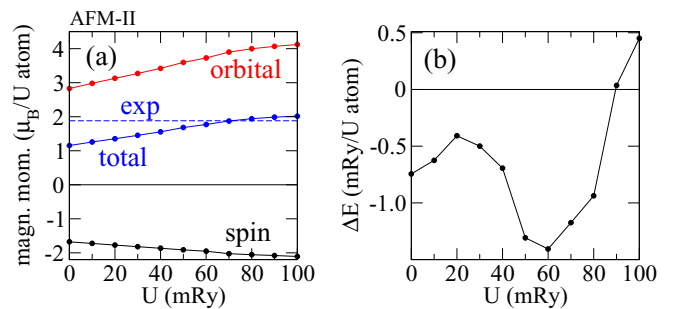


FIG. 3. (a) Spin, orbital, and total magnetic moments of the uranium atoms in the $(+ - - +)$ state as functions of parameter U of the LDA+ U method. Broken horizontal line shows the experimental value of the atomic moment. (b) Energy difference between $(+ - - +)$ and $(+ + + -)$ states as a function of U . The calculations are performed for the ambient lattice parameters.

values in the interval from 60 to 100 mRy. The U dependence of the energy difference $\Delta E = E_{\text{AFM-I}} - E_{\text{AFM-II}}$ is nonmonotonic. For $U > 90$ mRy the AFM-II structure is the lowest in energy in correspondence with the experiment. The energies of other three collinear states are distinctly higher than the energies of the competing AFM-I and AFM-II states and have the following values in the case of $U = 90$ mRy: 0.425, 0.504, and 1.033 mRy/ U where all energies are counted from the energy of the AFM-II state. So, the account for on-site electron correlations within the LDA+ U method improves the agreement with experiment concerning both the value of the atomic moment and the competition of the energies of the AFM-II and AFM-I structures.

B. Magnetic structures collinear to the c axis for reduced volume

Aiming to understand the physical nature of the pressure-induced AFM-FM transition we performed calculations of the collinear structures considered in Sec. III A for the reduced crystal volume. We expected that the energy distance between AFM and FM states will decrease with decreasing volume and will become zero at a certain critical volume. We did not, however, obtain such a behavior. In this paper we will discuss calculations performed for the lattice parameter reduced by 5%. The energy of the FM state remained distinctly higher than the energy of the AFM-II state. The energy difference of these two states varied between 0.894 and 1.264 mRy/ U for U varying between 70 and 100 mRy.

To understand the reason for this apparent disagreement with the experimental observation of the pressure-induced phase transition we need a more detailed insight into magnetic interactions than the information provided by the calculations of few magnetic states with atomic moments collinear to the c axis. Therefore, in the next step we considerably increase the number of calculated magnetic states.

The following new types of the magnetic states will be included into consideration. First, to study the properties of the MA we calculate collinear magnetic states with atomic moments aligned along various directions in the crystallographic ac plane. Second, we perform calculations for selected noncollinear states aiming to obtain more detailed information on the interatomic exchange interactions.

C. Magnetic anisotropy properties

We continue with the study of the MA. This is achieved through the evaluation of the energies of the magnetic configurations obtained by the rigid rotation of selected magnetic states within the ac plane. In these calculations the relative directions of the atomic moments remain unchanged and only the orientation of the moments with respect to the crystallographic axes is varied. Under the assumption of the single-ion type of the MA, common for all magnetic structures, similar properties of the energy $E(\theta)$ for different collinear magnetic configurations should be expected. Here θ is the rotation angle measured from the c axis. In striking contrast to this expectation, the LDA calculations give very different results for the FM and AFM configurations [Figs. 4(a)–4(d)]. For both AFM-I and AFM-II structures the $E(\theta)$ dependence corresponds well to the picture of single-ion MA: $E(\theta)$ has

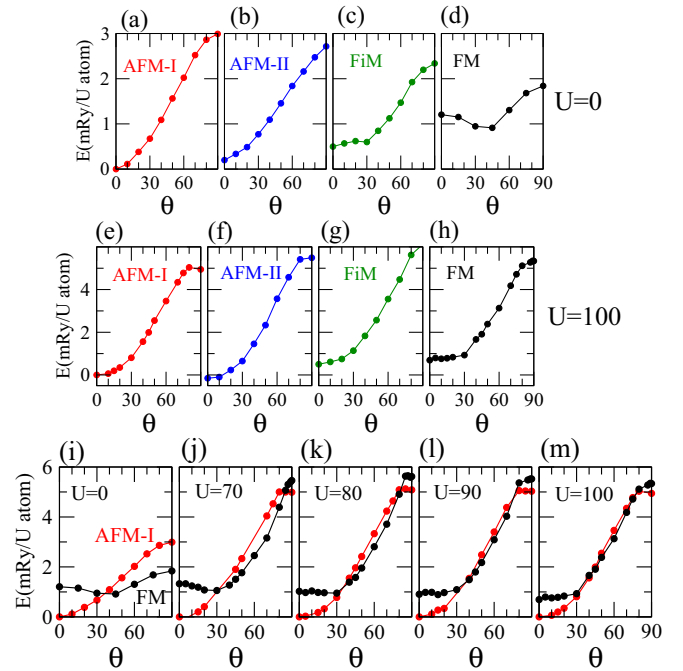


FIG. 4. Energies of magnetic states as functions of angle θ counted from the c axis. All calculations are performed for ambient lattice parameters. (a)–(d) $U = 0$ (LDA) calculations for magnetic structures (+ - + -), (+ - - +), (+ + + -), (+ + + +), respectively. (e)–(h) The same as in (a)–(d) but for $U = 100$ mRy. (i)–(n) The comparison of the $E(\theta)$ curves of AFM-I and FM structures calculated for various values of parameter U . The values of U are given in mRy.

the form close to a simple cosine-type function [Figs. 4(a) and 4(b)]. In contrast to the AFM-I and AFM-II cases, the calculation for the FM structure gives much weaker energy variation and the energy minimum at an intermediate direction between crystallographic c and a axes [Fig. 4(d)] [37]. The shape and the energy position of the $E(\theta)$ curve for FiM structure [Fig. 4(c)] is intermediate between corresponding curves for the AFM and FM structures.

The peculiar behavior of the FM $E(\theta)$ [Fig. 4(d)] indicates the importance of the interlayer hybridization. Since the positions of the Sb atoms in the layers above and below a U atom are shifted in the ab plane with respect to the layers of the U atoms, the lines connecting a U atom with nearest Sb atoms are not collinear to the c axis (Fig. 1). Also the U atoms of adjacent U layers are shifted with respect to each other in the ab planes. The strong electron hybridization along the lines connecting nearest atoms can result in the magnetic easy axis deviating from the c axis. We remark that in this case the symmetry of the crystal leads to the presence of equivalent domains with different directions of the deviation of the magnetization from the c axis. Because of this symmetry, the average magnetization of all domains with positive projections of the magnetization on the c axis will be parallel to the c axis. However, microscopically it is of crucial importance that the minimum energy corresponds to the magnetic configuration with canted moments. This result showing the importance of the interlayer hybridization is in

correlation with the experimental conclusion [12] that the electronic structure of USB_2 should not be treated as a purely 2D one.

Since, as discussed above, the LDA does not describe correctly the ground state of USB_2 we performed calculations of the $E(\theta)$ curves also with the LDA+ U method. The obtained changes of the $E(\theta)$ dependencies are large. In Figs. 4(e)–4(h), we present the $E(\theta)$ curves for the same magnetic structures calculated with the LDA+ U method and $U = 100$ mRy. In this case the difference between $E(\theta)$ curves for the AFM and FM structures becomes much smaller. All four curves are now closer to each other and to the simple cosine-type form. The amplitudes of the curves are also rather similar. There is however a remarkable flat part in the low- θ region of the FM curve [Fig. 4(h)]. In Figs. 4(i)–4(m) we compare the AFM-I and FM curves calculated for different U values. For $U = 70$ mRy, the FM curve is slightly nonmonotonic with minimum at $\theta \sim 30^\circ$ [Fig. 4(h)]. The minimum becomes very shallow for $U = 80$ mRy [Fig. 4(i)] and disappears with further increase of U [Figs. 4(j) and 4(k)]. What remains is the flat part of the curve in the low- θ region mentioned above.

It is worth commenting here on the origin of the obtained strong dependence of the MA properties on the magnetic configuration and value of parameter U . The reason for this dependence is the dependence of the electronic structure on the magnetic configuration and the value of U . The function $E(\theta)$ is an integral characteristic of the changes in the electronic structure caused by the variation of angle θ . The contributions to the $E(\theta)$ from different parts of the electronic spectrum differ in both sign and value that makes the MA properties a sensitive result of the complex balance of strongly compensating each other contributions. The change of the electronic structure due to the change of the magnetic configuration and/or U value influences the balance of contributions and results in different $E(\theta)$ dependence. Therefore the properties of the $E(\theta)$ function cannot be predicted without direct numerical calculation. Because of this, we do not suggest a qualitative interpretation of the particular features of the $E(\theta)$ curves treating them as “accidental” consequences of the complex changes of the electron structure.

To address the high-pressure experiment we performed calculations of $E(\theta)$ for reduced volume (Fig. 5). A striking property of the results is reappearance of distinct

nonmonotonic behavior of $E(\theta)$ in the case of FM structure. Now it is, however, the feature of the MA obtained with the LDA+ U method. Because of the nonmonotonic character of the FM curve the energy minimum is shifted from $\theta = 0$ corresponding to the c axis to an accidental θ value. With account for this property we obtain expected competition between the energies of the AFM and FM states. These calculations suggest that the competition of the energies of the FM and AFM states revealed by the high-pressure experiment cannot be understood if only the magnetic configurations collinear to the c axis are considered. The position of the minimum of the FM curve with respect to the minimum of the AFM curve depends on the U value. For $U = 100$ mRy, the minimum of the FM structure is higher. However, with decrease of the U value to 80 and 70 mRy the relative positions of the minima change to the opposite. This means that a trend to better correlation with pressure experiment is obtained for values of U decreasing with pressure. This trend seems to be physically plausible since the smaller lattice parameter leading to increased delocalization of the $5f$ electrons results in decreasing on-site electron correlation and therefore smaller U value.

We emphasize that it is just the FM energy becoming lower than the AFM energy with decreasing volume and not the FiM energy. In Fig. 5 we present $E(\theta)$ curves for the FiM structure. Although, for the $\theta = 0$ the FiM state is lower in energy than the FM one, with account for nonzero θ the FM energy becomes distinctly lower.

D. Discontinuous change of the magnetic critical temperature

Our next goal is to understand the physical origin of the strong drop of the magnetic critical temperature after the pressure-induced AFM-FM transition. In general, the critical temperature of a given phase of the system depends on the magnetic excitations of this state. Among characteristics determining the properties of magnetic excitations are interatomic exchange interactions.

The purpose of this section is to perform estimations of the exchange interactions between layers of the uranium atoms and, on this basis, to discuss the features leading to the observed pressure dependence of the magnetic critical temperature.

1. Interlayer exchange parameters through the energies of the collinear magnetic states

First, we will discuss the estimation of the exchange parameters based on the energies of the four magnetic configurations (+ − − +), (+ − + −), (+ + − −), and (+ + + +) with atomic moments collinear to the c axis. In each of these four magnetic states the uranium atoms are equivalent to each other. We consider the model Hamiltonian

$$H = - \sum_{ij} J_{ij} \mathbf{e}_i \cdot \mathbf{e}_j, \quad (1)$$

where J_{ij} are parameters of the exchange interaction between atomic layers i and j ; \mathbf{e}_i is the unit vector in the direction of the atomic moments of layer i [38]. The differences of the

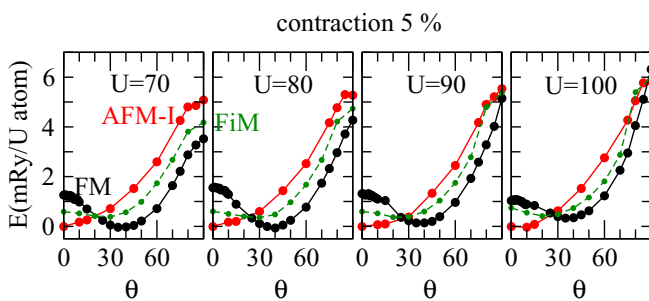


FIG. 5. Energies of AFM-I (red), FM (black), and FiM (green) states as functions of angle θ . The calculations are performed for contracted lattice with different values of parameter U : (a) 70 mRy, (b) 80 mRy, (c) 90 mRy, (d) 100 mRy.

energies of the four magnetic states calculated per magnetic unit cell with four U atoms (Fig. 1) are

$$E_2 - E_1 = 8(J_2 - 2J_3), \quad (2)$$

$$E_3 - E_1 = -8(J_1 - J_2), \quad (3)$$

$$E_4 - E_1 = -8(J_1 + J_3). \quad (4)$$

The interlayer exchange parameters J_1, J_2, J_3 are defined in Fig. 1. Equations (1)–(4) assume that the energy differences of the magnetic states are solely due to the exchange interaction. Since the low-energy magnetic structures are antiferromagnetic it is expected that the exchange parameters estimated according to Eqs. (2)–(4) are predominantly of the AFM type. Indeed, all three parameters appear to be negative. For the LDA calculation ($U = 0$) we get the following values of the parameters: $J_1 = -0.40$ mRy, $J_2 = -0.17$ mRy, $J_3 = -0.04$ mRy. For $U = 90$ mRy, we get $J_1 = -0.36$ mRy, $J_2 = -0.15$ mRy, $J_3 = -0.08$ mRy. The relative stability of the AFM-II and AFM-I structures depends, according to Eq. (2), on the sign of the difference ($J_2 - 2J_3$).

The exchange parameters determined in this section reproduce the energy differences of several collinear magnetic states. However, it is not obvious that these parameters can be used to estimate the energies of the magnetic excitations about any of the collinear states involved in the estimation. We need to carry out the calculations that provide the exchange parameters characterizing the excitations about AFM-II and FM states since the critical temperatures of these two states are the quantities we are interested in. Such calculations are discussed in the next section.

2. Exchange parameters through the energies of small deviations of atomic moments

The calculations are performed as follows. We chose as a reference state the collinear configuration we are going to study and estimate the exchange parameters corresponding to this state by evaluating the energies of the deviations of the

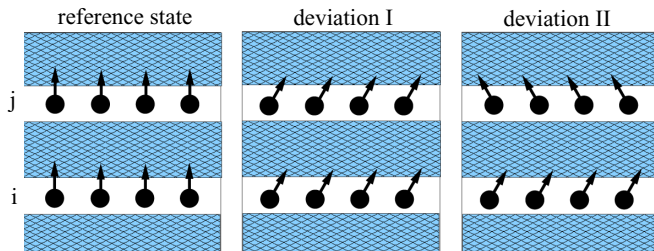


FIG. 6. Schematic presentation of the magnetic configurations used in the estimation of the exchange parameters between i th and j th layers. Left: Reference state whose exchange interactions are studied. Only i th and j th layers are distinguished. The rest of the system is shown by shaded areas. Middle: The atomic moments of the i th and j th layers deviate by the same angle and in the same direction. The directions of the atomic moments in the rest of the system remain unchanged. Right: The atomic moments of the i th and j th layers deviate by the same angle but in the opposite directions. The directions of the atomic moments in the rest of the system remain unchanged.

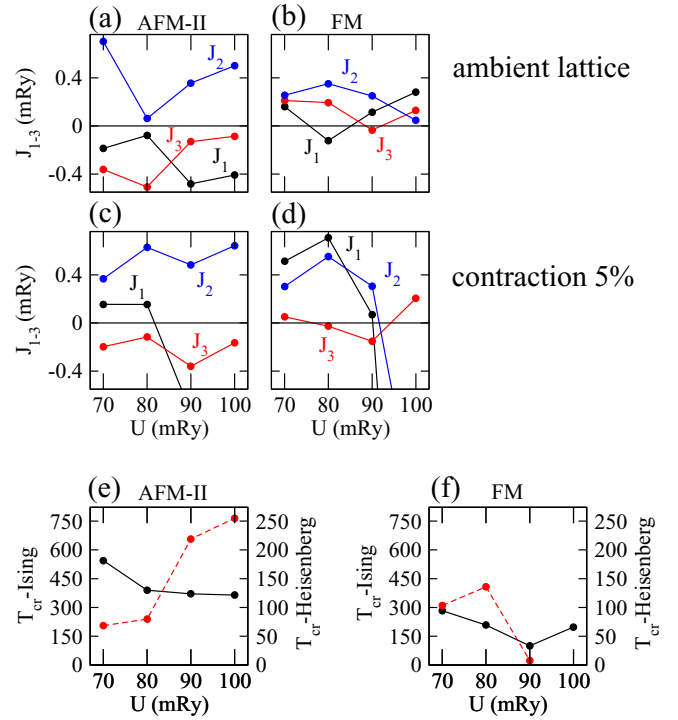


FIG. 7. (a) Exchange parameters $J_1, J_2,$ and J_3 as functions of parameter U calculated for AFM-II state and ambient lattice parameter. (b) The same as (a) but for the FM structure. (c) The same as (a) but for contracted lattice. (d) The same as (b) but for contracted lattice. (e) The mean-field estimation of the magnetic critical temperature as a function of U for the AFM-II structure for both ambient (solid black line) and contracted (red broken line) lattices. The left-side scale of the ordinate axis gives the critical temperature estimated for the Ising model. The right-side scale of the ordinate axis gives the critical temperature estimated for the Heisenberg model. (f) The same as (e) but for the FM structure.

atomic moments from this state. To estimate the exchange parameter J_{ij} for the pair of U layers (i, j) we perform calculations of two noncollinear configurations, shown schematically in Fig. 6. In the first configuration, the magnetic moments of both i th and j th layers deviate within the ac plane in the same direction (middle panel of Fig. 6). Therefore in this case the moments of the i th and j th layers remain collinear to each other but become noncollinear to the moments of other layers. In the second configuration, the deviation directions for the i th and j th layers are opposite (right panel of Fig. 6). The deviation angle has in both cases the same value. We assume that the anisotropy energies connected with the deviations of the moments are approximately equal for the two configurations and the difference of the energies of these configurations provides an estimation of the exchange parameter J_{ij} ,

$$J_{ij} = \frac{1}{2}(E_{II} - E_I)/[1 - \cos(2\theta)]. \quad (5)$$

In Figs. 7(a)–7(d) we present the exchange parameters for AFM-II and FM configurations calculated for four values of parameter U and both ambient and contracted lattices. In all calculations we used deviation angle $\theta = 20^\circ$. The comparison of Figs. 7(a) and 7(b) shows that the exchange parameters calculated for AFM-II and FM structures at ambient volume

are principally different. Even the signs of the interactions do not coincide. We also see that these parameters differ from the parameters obtained in Sec. III D 1 by comparing the energies of few collinear configurations. Obviously, the parameters reproducing the relative energies of several collinear states do not describe the small-angle excitations of any of these states and cannot be used for the estimation of the magnetic critical temperature of these states.

The strong difference of the exchange parameters obtained using the energies of different magnetic configurations is explained by the fact that we deal with a complex many-electron system and not with an ideal Heisenberg magnet, all magnetic configurations of which are described by one and the same set of the interatomic exchange parameters.

Consideration of the exchange parameters obtained for contracted lattice [Figs. 7(c) and 7(d)] shows again a large difference between AFM-II and FM structures. Also the exchange parameters calculated for the same structure but different volumes differ strongly from each other, which is another demonstration of the sensitivity of the exchange parameters to the change in the electronic structure caused by the change of magnetic configuration, volume, or parameter U .

The analysis of Figs. 7(a)–7(d) shows that the complex character of the U and volume dependencies of the individual exchange parameters does not allow us to establish any clear general trends. In the next step, we will consider the more integral quantity

$$J_0 = \sum_{i=2,3,4} J_{1i}(\mathbf{e}_1 \cdot \mathbf{e}_i) \quad (6)$$

that determines effective exchange field acting on the atomic moments. This quantity allows us to make a rough estimate of the magnetic critical temperature by applying the mean-field-type formula

$$T_{\text{cr}} = cJ_0/k_B, \quad (7)$$

where $c = 1$ for the Ising model and $c = \frac{1}{3}$ for the Heisenberg model. The Ising model can be considered as a limit of infinitely strong uniaxial anisotropy. In contrast, the Heisenberg's expression corresponds to negligible MA. The property that stronger MA leads to larger critical temperature is well known (see, e.g., Ref. [39]). The physical background of this property is a decreased number of the low-energy excitations in the strongly anisotropic systems.

In Figs. 7(e) and 7(f) we present the magnetic critical temperatures calculated with Eq. (7) for both AFM-II [Fig. 7(e)] and FM [Fig. 7(f)] structures and for both Ising and Heisenberg models. The same value of J_0 was used for both models. The calculations are performed for four values of parameter U and two values of crystal volume. The consideration of the blue line in Fig. 7(e) corresponding to the AFM-II structure of ambient lattice shows that the Ising model overestimates the value of the critical temperature whereas the Heisenberg model underestimates its value. Obviously, although the MA of the system plays an important role, USb_2 should not be treated as an Ising system with infinitely strong MA.

The results for the AFM-II structure presented in Fig. 7(e) show that for U equal to 70 and 80 mRy the decreased volume leads to decreased J_0 and, correspondingly, decreased T_{cr} . For U equal to 90 and 100 mRy, the trend is opposite.

This demonstrates that the magnetic critical temperatures of the uranium compounds can, in general, both decrease and increase with applied pressure. In our calculations discussed in Sec. III A the U values of 90 and 100 mRy give the best agreement with experiment concerning the description of the AFM ground state. Therefore the trend obtained for these values of U seems to be more relevant. This trend correlates with the experimental observation of increasing Néel temperature of the AFM-II structure with increasing pressure [9].

The analysis of Fig. 7(f) shows that in the case of the FM structure the trend in the variation of the critical temperature with decreasing volume is opposite to the AFM-II case. Here, for U equal to 70 and 80 mRy T_c increases somewhat and for 90 and 100 mRy it decreases. For $U = 100$ mRy the decrease is very strong and the estimation of T_c becomes negative indicating the instability of the FM state. This result in combination with the results of Sec. III C lead to the conclusion that for the reduced volume $U = 70$ mRy gives a more adequate description of the trends concerning the phase transition to the FM state. We conclude that to describe the pressure induced transition to the FM state the decrease of U with decreasing volume should be taken into account. In the case of $U = 70$ mRy the Heisenberg model shows good performance giving the Curie temperature close to 100 K.

In general the critical temperature of the AFM-II structure [Fig. 7(e)] is higher than the corresponding temperature of the FM structure [Fig. 7(f)] that correlates well with the experimental result. In addition, our calculations discussed in Sec. III C have shown that there is a trend that the MA of the AFM structure is larger than the MA of the FM structure. Since larger anisotropy leads to larger magnetic critical temperature this is an additional factor explaining the distinctly smaller critical temperature of the FM state compared to the AFM state.

E. Calculations with external magnetic field

To address the AFM-FiM phase transition obtained in the in-field experiment we carried out the calculations with applied magnetic field (see Fig. 8). The questions we want to answer are the following: First, do our calculations support the existence of the in-field transition from the AFM-II structure to the FiM for the field strength close to the experimental value [10]? In this case we deal with the competition of the in-field energy of the FiM structure and the energy of the AFM ground state.

The second question is closely related to the first one: Why does the field-induced transition bring the system to the FiM state and not to the FM state where the effect of the Zeeman interaction with the field is expected to be about two times larger? Indeed, in the FiM structure there are two uncompensated U moments per supercell while in the FM structure this is four atomic moments.

Since the in-field transition is observed at the ambient pressure, to answer this question we compare the energies of the FiM and FM states calculated for the ambient lattice parameters. We will discuss calculations performed with parameter $U = 90$ mRy. As we have seen, this value of U gives good agreement with experiment concerning both the ground-state magnetic structure and the value of the uranium

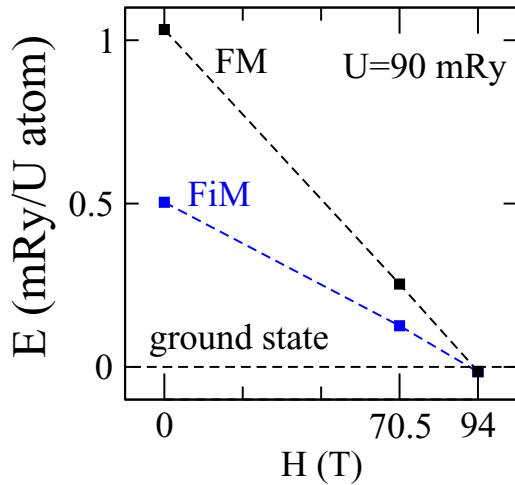


FIG. 8. Energies of FiM and FM configurations in applied magnetic field. The energy origin is at the energy of the antiferromagnetic ground state.

atomic moment. We consider the results of the calculations for applied fields of 70.5 and 94 T. These fields correspond to the Zeeman energies of the unit magnetic moment of $1\mu_B$ equal to 0.3 and 0.4 mRy, respectively. These values of the field are reasonably close to the experimental value of the low-temperature magnetic critical field. (For temperature of 80 K the measured magnetic critical field is 63 T [10]. For 0 K the critical field is expected to increase somewhat.)

It is important to notice that the calculations without applied magnetic field gave the energy of the FiM state to be lower by 0.53 mRy/U atom than the energy of the FM state. In-field calculations, as expected, result in the lowering of the energies of both FiM and FM states with the energy of the FM structure decreasing faster. However the large energy difference of the FiM and FM structures at the ambient conditions is the reason why the energy of the FiM structure remains lower than the energy of the FM structure up to rather large applied fields.

Our calculations show that the FiM state remains lower in energy up to a field value of about 95 T. This field is above the experimental critical field. This result supports the experimental conclusion that the in-field transition takes place to the FiM state. We also see that the energy of the in-field FiM and FM structures reaches the energy of the AFM ground state at about the same field strength that is higher than the experimental critical field of about 70 T. Obviously this relation between energies of the magnetic states predicts the in-field transition at somewhat larger field than experimental critical field. We remark, however, that it should not be expected that our physical model will quantitatively reproduce the whole

complexity of the competition between properties of several different magnetic configurations.

IV. CONCLUSIONS

This work was stimulated by recent experiments revealing pressure induced transition from the ground-state antiferromagnetic structure to the ferromagnetic structure and magnetic field-induced transition to the ferrimagnetic structure. Remarkably, the magnetic critical temperature of the FM state, induced by pressure, is more than two times smaller than the Néel temperature of the AFM ground state. We performed LDA and LDA+ U studies to reveal the origin of the unusual (+ - -+) magnetic ground state of the system and the driving mechanisms of the phase transitions.

We show that the use of the LDA+ U method is necessary to describe properly the competition between (+ - -+) and (+ - +-) states and obtain the value of the U magnetic moment close to the experimental value.

To study pressure-induced effects we carry out calculations for reduced volume and demonstrate that the energy of the FM state indeed becomes lower than the energy of the AFM state. However, this feature depends crucially on the peculiar features of the magnetic anisotropy: the easy axis of the FM state deviates from the high-symmetry crystallographic c axis.

We calculate interlayer exchange parameters and estimate corresponding magnetic critical temperatures of the Ising and Heisenberg models. We show that the value of the critical temperature can both increase and decrease with decreasing lattice volume depending on the value of parameter U . For the (+ - -+) structure and $U = 90$ mRy and $U = 100$ mRy, T_{cr} increases with decreasing volume that correlates with the experimental behavior of the (+ - -+) phase. In agreement with experiment we obtained that the estimated exchange parameters of the FM phase give in general a smaller value of the critical temperature than for the (+ - -+) state. In combination with the revealed trend to a weaker MA of the FM state we obtain strong arguments in favor of distinctly lower critical temperature of the FM phase obtained experimentally.

We performed calculations with applied magnetic field and demonstrate that for the field of $H = 70.5$ T, close to the experimental critical field, the energy of the FiM state is lower than the energy of the FM state although the magnitude of the Zeeman energy of the FM is larger.

In general, our calculations reveal a number of important trends in the dependence of physical quantities on parameter U , volume, and magnetic field. In many cases we obtain competition of different trends that correlates with the variety of experimental properties and explains the richness of the properties of the uranium compounds.

- [1] V. Sechovsky and L. Havela, in *Handbook of Magnetic Materials*, edited by K. H. Bushow (Elsevier, Amsterdam, 1998), p. 1.
- [2] Y. Baer, H. R. Ott, and K. Andres, *Solid State Commun.* **36**, 387 (1980).
- [3] J. Kitagawa and M. Ishikawa, *Solid State Commun.* **153**, 76 (2013).

- [4] F. Lévy, I. Sheikin, B. Grenier, and A. D. Huxley, *Science* **309**, 1343 (2005).
- [5] W. Knafo, F. Duc, F. Bourdarot, K. Kuwahara, H. Nojiri, D. Aoki, J. Billette, P. Frings, X. Tonon, E. Lelièvre-Berna, J. Flouquet, and L.-P. Regnault, *Nat. Commun.* **7**, 13075 (2016).

- [6] J. Valenta, F. Honda, M. Valiska, P. Opletal, J. Kastil, M. Mísek, M. Divis, L. Sandratskii, J. Prchal, and V. Sechovsky, *Phys. Rev. B* **97**, 144423 (2018).
- [7] J. Pospíšil, Y. Haga, Y. Kohama, A. Miyake, S. Kambe, N. Tateiwa, M. Valiska, P. Proschek, J. Prokleska, V. Sechovsky, M. Tokunaga, K. Kindo, A. Matsuo, and E. Yamamoto, *Phys. Rev. B* **98**, 014430 (2018).
- [8] J. Pospíšil, J. Gouchi, Y. Haga, F. Honda, Y. Uwatoko, N. Tateiwa, S. Kambe, S. Nagasaki, Y. Homma, and E. Yamamoto, *J. Phys. Soc. Jpn.* **86**, 044709 (2017).
- [9] J. R. Jeffries, R. L. Stillwell, S. T. Weir, Y. K. Vohra, and N. P. Butch, *Phys. Rev. B* **93**, 184406 (2016).
- [10] R. L. Stillwell, I.-L. Liu, N. Harrison, M. Jaime, J. R. Jeffries, and N. P. Butch, *Phys. Rev. B* **95**, 014414 (2017).
- [11] J. Leciejewicz, R. Troc, A. Murasik, and A. Zygmunt, *Phys. Status Solidi* **22**, 517 (1967); **24**, 763(E) (1967).
- [12] E. Guziewicz, T. Durakiewicz, M. T. Butterfield, C. G. Olson, J. J. Joyce, A. J. Arko, J. L. Sarrao, D. P. Moore, and L. Morales, *Phys. Rev. B* **69**, 045102 (2004).
- [13] D. Aoki, P. Wisniewski, K. Miyake, N. Watanabe, Y. Inada, R. Settai, E. Yamamoto, Y. Haga, and Y. Onuki, *Philos. Mag. B* **80**, 1517 (2000).
- [14] D. Aoki, P. Wisniewski, K. Miyake, N. Watanabe, Y. Inada, R. Settai, E. Yamamoto, Y. Haga, and Y. Onuki, *J. Phys. Soc. Jpn.* **68**, 2182 (1999).
- [15] S. Lebegue, P. M. Oppeneer, and O. Eriksson, *Phys. Rev. B* **73**, 045119 (2006).
- [16] T. Durakiewicz, P. S. Riseborough, C. G. Olson, J. J. Joyce, P. M. Oppeneer, S. Elgazzar, E. D. Bauer, J. L. Sarrao, E. Guziewicz, D. P. Moore, M. T. Butterfield, and K. S. Graham, *Europhys. Lett.* **84**, 37003 (2008).
- [17] M. M. Wysokinski, *Phys. Rev. B* **97**, 041107 (2018).
- [18] Everywhere in the paper, the ambient lattice means the lattice with experimental lattice parameters at ambient conditions.
- [19] A. R. Williams, J. Kübler, and C. D. Gelatt, *Phys. Rev. B* **19**, 6094 (1979).
- [20] V. Eyert, *The Augmented Spherical Wave Method*, Lecture Notes in Physics (Springer-Verlag, Berlin, 2012), Vol. 849.
- [21] L. M. Sandratskii, *Adv. Phys.* **47**, 91 (1998).
- [22] L. M. Sandratskii, *Phys. Rev. B* **94**, 184414 (2016).
- [23] U. von Barth and L. Hedin, *J. Phys. C* **5**, 1629 (1972).
- [24] V. I. Anisimov, J. Zaanen, and O. K. Andersen, *Phys. Rev. B* **44**, 943 (1991).
- [25] V. I. Anisimov, F. Aryasetiawan, and A. I. Lichtenstein, *J. Phys.: Condens. Matter* **9**, 767 (1997).
- [26] An even more advanced method to account for on-site electronic correlations is LDA plus dynamical mean-field theory (LDA+DMFT) [see, e.g., G. Kotliar, S. Y. Savrasov, K. Haule, V. S. Oudovenko, O. Parcollet, and C. A. Marianetti, *Rev. Mod. Phys.* **78**, 865 (2006)]. The complexity of the LDA+DMFT scheme does not allow us to perform the study of the energetics of magnetic states of USb_2 reported in the paper. On the other hand, the long-term successful history of the applications of the LDA+ U method allows us to consider it as a reliable tool for the study of total energies and atomic magnetic moments of the magnetic states of USb_2 .
- [27] M. S. S. Brooks, *Physica B* **130**, 6 (1985).
- [28] M. R. Norman, *Phys. Rev. Lett.* **64**, 1162 (1990).
- [29] O. Eriksson, B. Johansson, and M. S. S. Brooks, *J. Phys.: Condens. Matter* **1**, 4005 (1989).
- [30] O. Eriksson, M. S. S. Brooks, and B. Johansson, *Phys. Rev. B* **41**, 7311(R) (1990).
- [31] L. Severin, L. Nordström, M. S. S. Brooks, and B. Johansson, *Phys. Rev. B* **44**, 9392 (1991).
- [32] B. Nonas, I. Cabria, R. Zeller, P. H. Dederichs, T. Hühne, and H. Ebert, *Phys. Rev. Lett.* **86**, 2146 (2001).
- [33] L. M. Sandratskii and J. Kübler, *Phys. Rev. Lett.* **75**, 946 (1995).
- [34] S. L. Dudarev, G. A. Botton, S. Y. Savrasov, C. J. Humphreys, and A. P. Sutton, *Phys. Rev. B* **57**, 1505 (1998).
- [35] A recent critical discussion of the DFT-based methods to account for the external magnetic field can be found in Ref. [36] and references therein.
- [36] S. Reimann, A. Borgoo, E. I. Tellgren, A. M. Teale, and T. Helgaker, *J. Chem. Theory Comput.* **13**, 4089 (2017).
- [37] It can be expected that in the case where the easy axis assumes an arbitrary direction [Fig. 4(d)] the U atomic moments become noncollinear. To verify this the self-consistent calculations of the magnetic structure were performed starting with arbitrary oriented U magnetic moments. If the U moments in the initial configuration had positive projections on the c axis the calculations converged to the magnetic configuration with the U moments oriented according to the energy minimum in Fig. 4(d). The angle between the U moments was below 0.1° . If the two moments in the initial configuration had opposite c projections the self-consistent magnetic structure was antiferromagnetic with moments collinear to the c axis. In the course of iterations the moments never changed the sign of the z projection. This is explained by high anisotropy energy of the atomic moments parallel to the ab plane playing the role of high-energy barrier.
- [38] It is worth commenting on the relation between the itinerancy of the electronic states and the formation of well-defined atomic moments assumed in Eq. (1). This very important question was extensively discussed in the scientific literature [see, e.g., T. Moriya, *Spin Fluctuations in Itinerant Electron Magnetism* (Springer, Berlin, 1985); B. L. Gyorffy, A. J. Pindor, J. Staunton, G. M. Stocks, and H. Winter, *J. Phys. F* **15**, 1337 (1985); V. P. Antropov, M. I. Katsnelson, B. N. Harmon, M. van Schilfgaarde, and D. Kusnezov, *Phys. Rev. B* **54**, 1019 (1996); Ref. [21]]. The Stoner theory that neglects the formation of the well-defined atomic moments and the low-energy transversal fluctuations of these moments failed by the order of magnitude in the estimation of the Curie temperature of the elementary itinerant ferromagnets (Fe, Co, Ni). The mapping of itinerant-electron magnets on the effective Hamiltonians of the interacting atomic moments is a powerful tool in the study of the thermodynamics of magnetic systems. The parameters of the effective Hamiltonian depend on the electronic structure and therefore on all interactions important for the formation of the electronic structure; among them are exchange interaction, spin-orbit interaction, and the value of parameter U .
- [39] Z. Siming, *J. Phys. Chem. Solids* **49**, 1419 (1988).